Supplementary Materials for

A supramolecular non-mesogenic route towards autonomous liquid crystal elastomer soft robots

Changfei He, Yufan Yang, Hong Wan, Ning Zheng, Yibao Li and Tao Xie
Corresponding to hechangfei@gnnu.edu.cn.; taoxie@zju.edu.cn

Table of contents

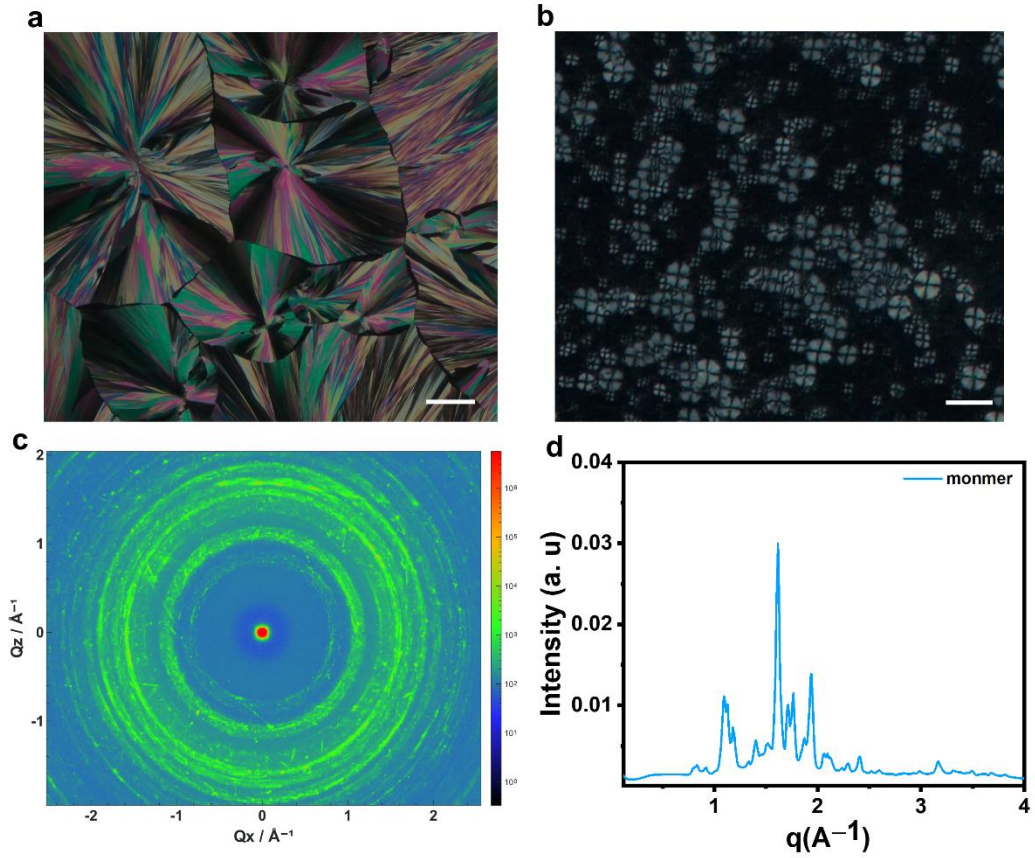

Supplementary Fig. 1 | Microstructure of oxime-ester-6 monomer and linear POE. POM images of **a,** Oxime ester-6 monomer, scar bar: 200 μm **b**, Linear POE-6, scar bar: 20 μm, after cooling from its melting temperature to 20 °C. **c**, 2D-WAXD images of oxime-ester-6 at 20 °C. **d**, 1D X-ray data derived from (**c**). As illustrated in the figure, during the cooling process, neither the monomer nor the linear POE exhibits any liquid crystal features. Instead, spherical crystals are observed, indicating that the structures do not transition into liquid crystalline states. From the WAXD results, it can be seen that oximer-ester-6 does not show laminar ordered scattering peaks in the small-angle region or short-range ordered π-π stacking peaks, instead, many narrow peaks (crystalline peaks) can be seen in the range of 1~3 A^{-1}. This rules out that the liquid crystal nature of oximer-etster-6.

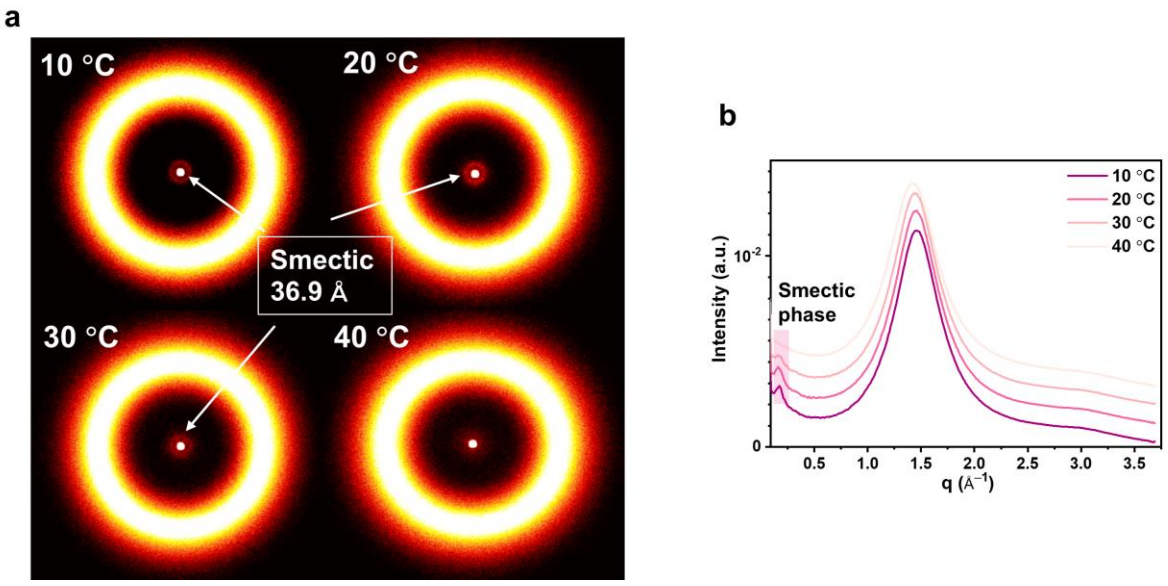

Supplementary Fig. 2 | Phase behavior of POE-6 with varying temperature. **a**, 2D WAXD images of POE-6 at different temperatures. **b**, 1D X-ray data derived from (a). The inner halo becomes darker with increasing temperature until it disappears at 40 ℃. The derived 1D XRD curves indicate that the intensity of the smaller peaks around 0.17 $Å^{-1}$ weakened progressively until disappearance. This suggests POE-6 experiences a transition from smectic to isotropic and the transition temperature is between 30 to 40 ℃.

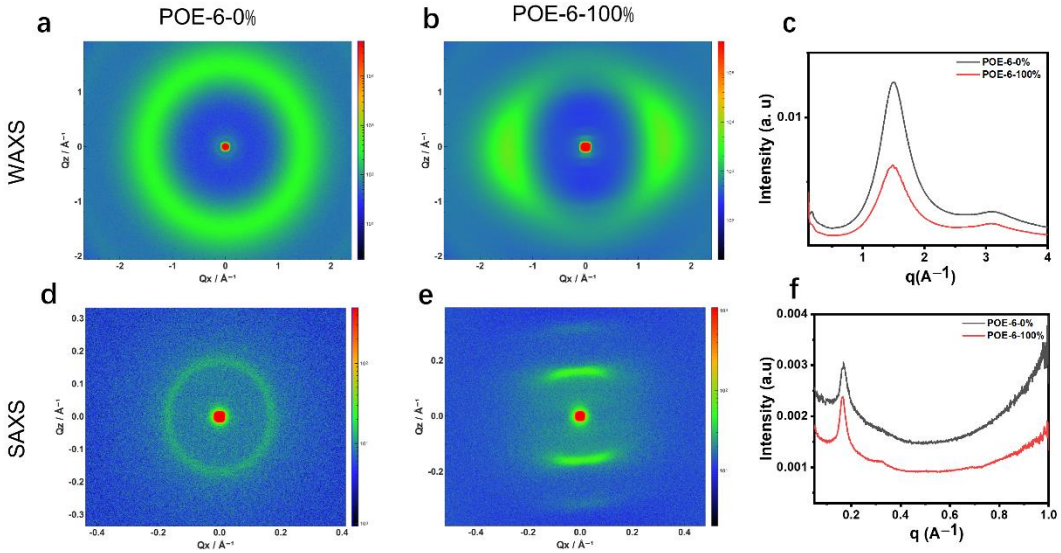

Supplementary Fig. 3 | WAXD/SAXS of polydomain and monodomain POE-6 at 20°C. WAXD images of polydomain POE-6 (**a**) and monodomain POE-6 (**b**). **c**, 1D X-ray data derived from (**a**) and (**b**). SAXS images of polydomain POE-6 (**c**) and monodomain POE-6 (**d**). **f**, 1D X-ray data derived from (**c**) and (**d**). Alignment was achieved by stretching the samples to 100% engineering strain before analysis. The stretching direction is perpendicular. Diffraction ring or arc observed in the small-angle region ($0.17A^{-1}$) of both 2D WAXD and 2D-SAXS images indicate the presence of smectic layered order in POE-6. After alignment, the small-angle scattering ring form two symmetrical arcs perpendicular to the stretching direction, further confirming that this smectic phase is the smectic A phase.

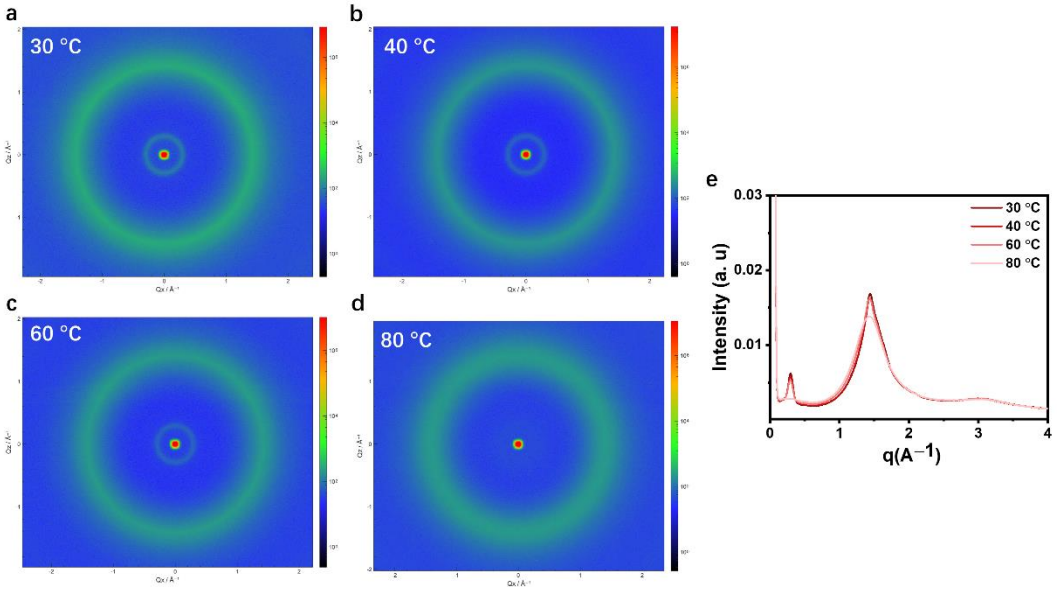

Supplementary Fig. 4 | Phase behavior of POE-12 with varying temperature. **a**-**d**, 2D WAXD images of POE-6 at different temperatures. **e**, 1D X-ray data derived from (**a**)-(**d**).

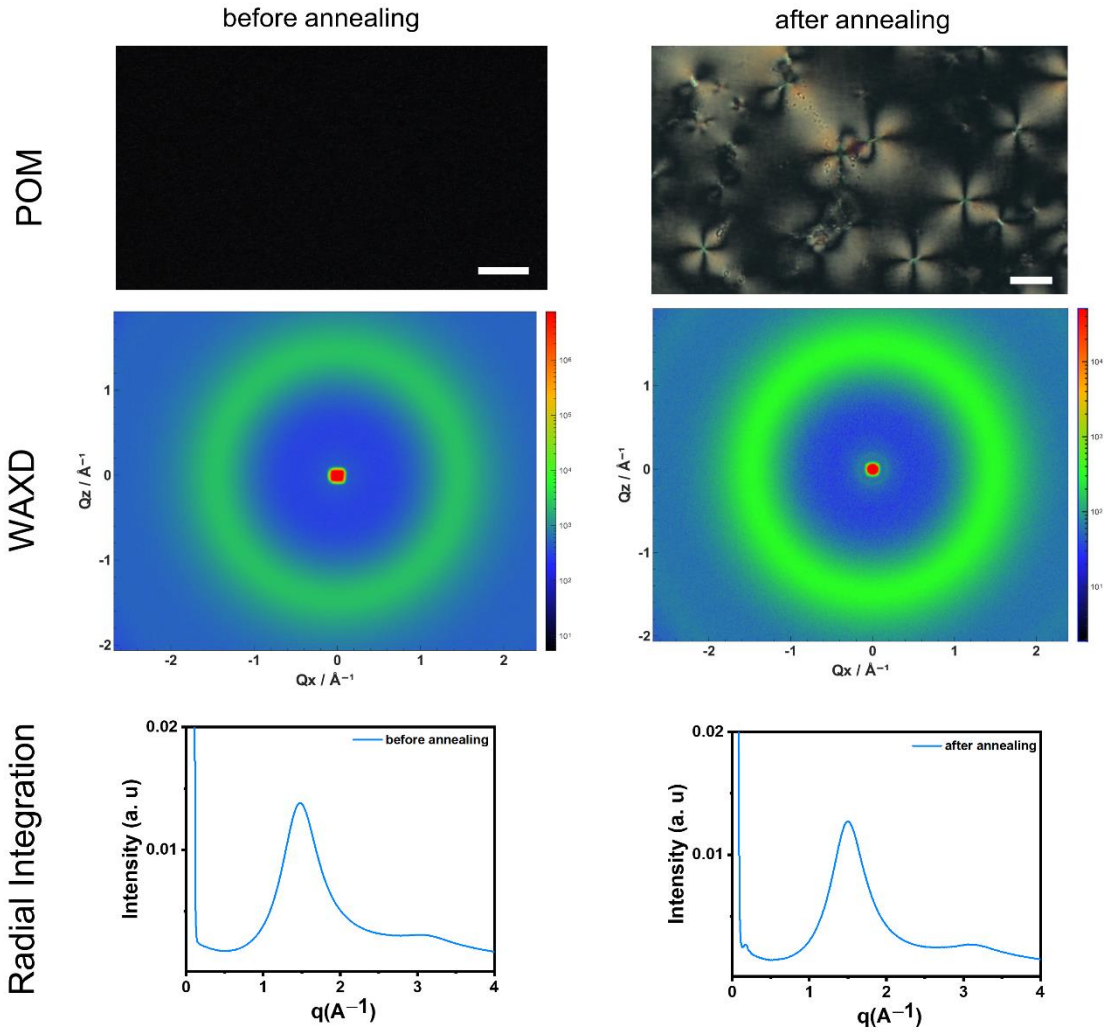

Supplementary Fig. 5 | POM images and WAXD patterns of POE-6 before and after annealing. The results reveal that no significant birefringence was observed in polarized light images prior to annealing. However, after annealing, abundant focal conic fan-shaped textures with well-defined four-brush (Maltese cross) extinction patterns became visible. Concurrently, WAXD analysis showed no diffraction rings in the smectic region before annealing. Following annealing, distinct diffraction rings appeared in the smectic region, indicating the formation of a layered, ordered smectic phase.

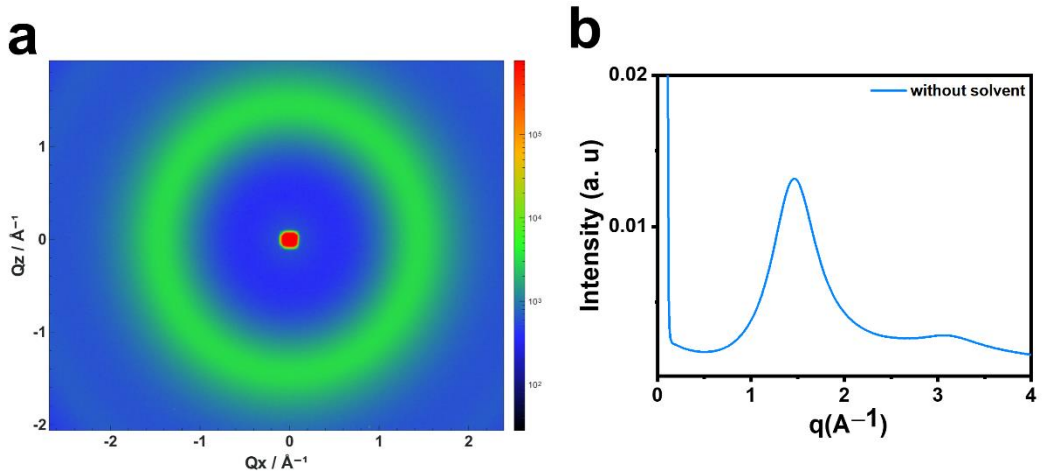

Supplementary Fig. 6| a, 2D WAXD pattern of polymerized POE-6 without solvent at 20 °C. **b,** 1D X-ray data derived from **(a).**

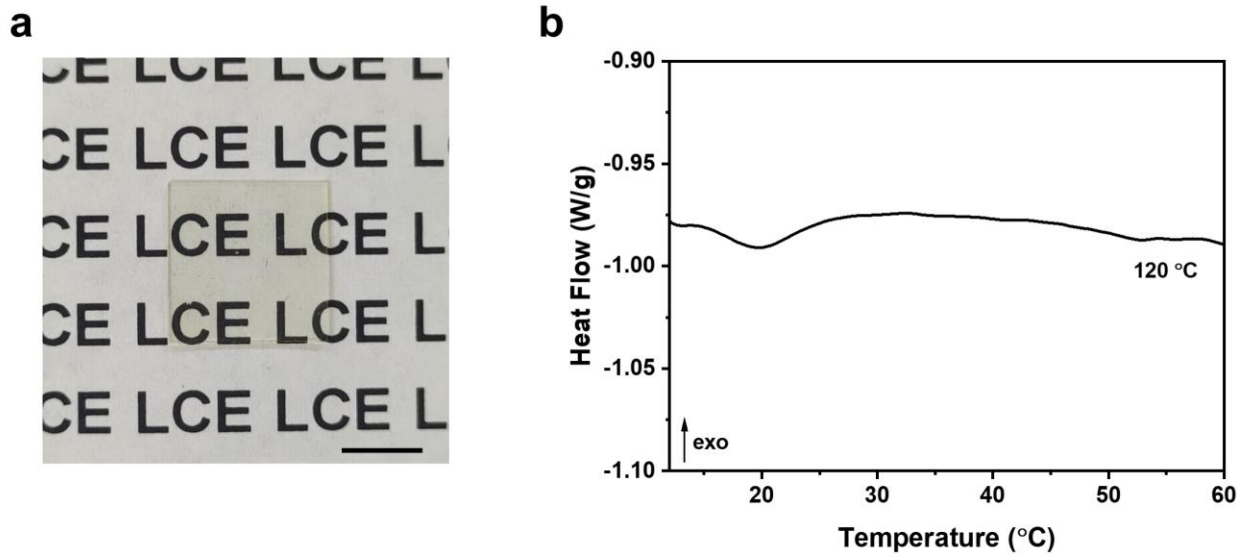

Supplementary Fig. 7 | Properties of POE-6 when annealing at 120 ℃ for 2 hours. **a,** Sample photo. **b**, DSC curve of POE-6 after annealing at 120 ℃ for 2 hours. Scale bar: 1 cm. The transparent appearance and the disappearance of the transformation peak on the DSC curve indicate that annealing at 120 ℃ results in failure to form a liquid crystalline phase.

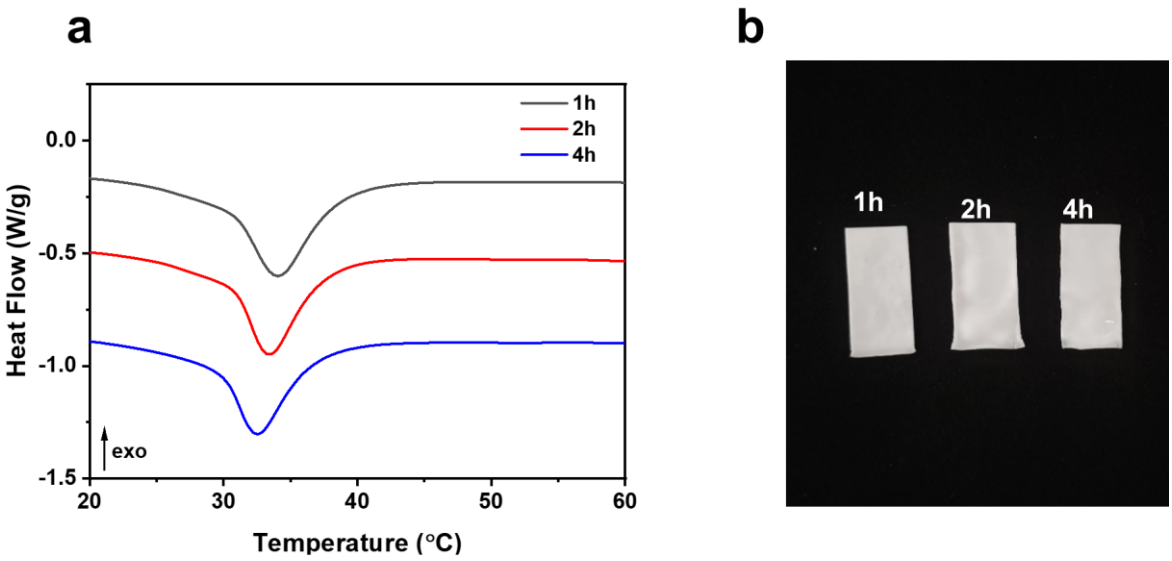

Supplementary Fig. 8 |. Property change of POE-6 with varying annealing time. **a**, DSC curves. **b**, photos of POE-6 after annealing at 80 °C for different times. Scale bar: 1 cm.

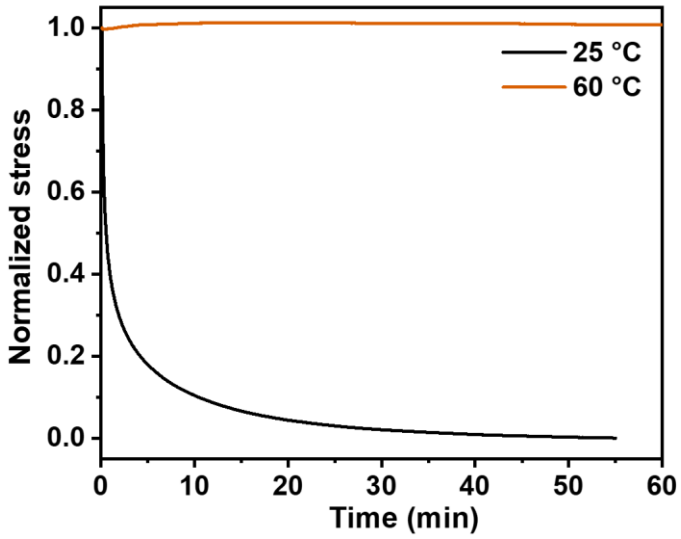

Supplementary Fig. 9 |. Stress relaxation curves of POE-6 at different temperature.

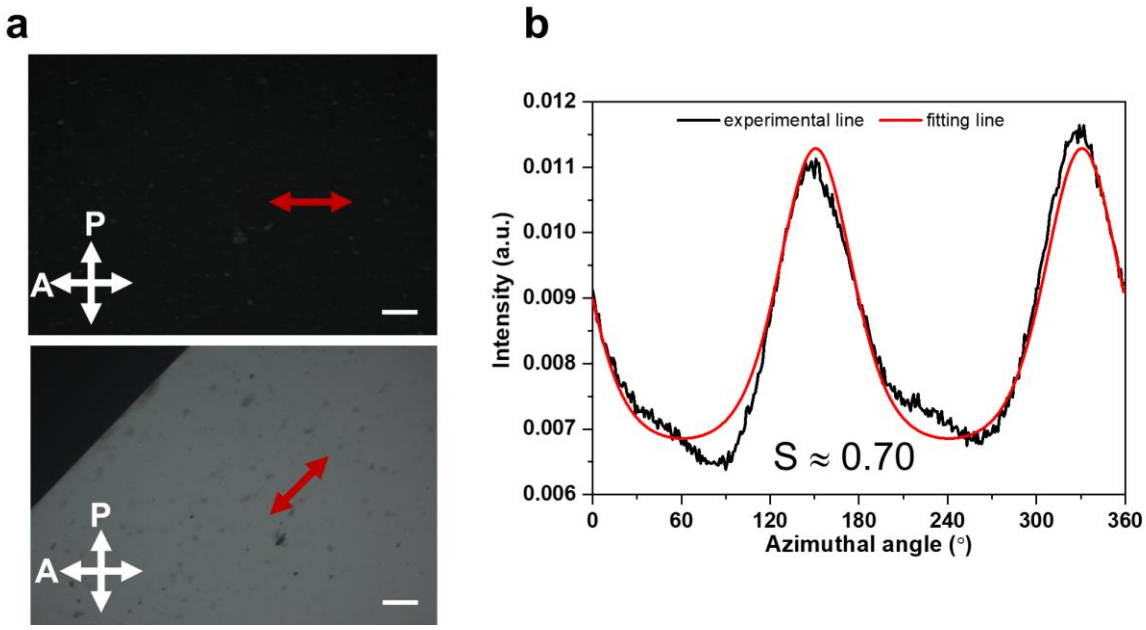

Supplementary Fig. 10 | Properties of the aligned POE-6. **a**, POM images of POE-6 stripe after programming (50% programming strain at 40 ℃ for 18h). **b**, Azimuthal intensity scan curves of POE-6. The degree of orientation (*S*) is taken according to the fitted equation and is calculated by the following equation[20]:

$$S = \frac{3 < \cos^2 \phi > -1}{2}$$

$$< \cos^2 \phi >= \frac{\int_0^{\frac{\pi}{2}} I(\phi) \sin\phi \cos^2\phi \, d\phi}{\int_0^{\frac{\pi}{2}} I(\phi) \sin\phi \, d\phi}$$

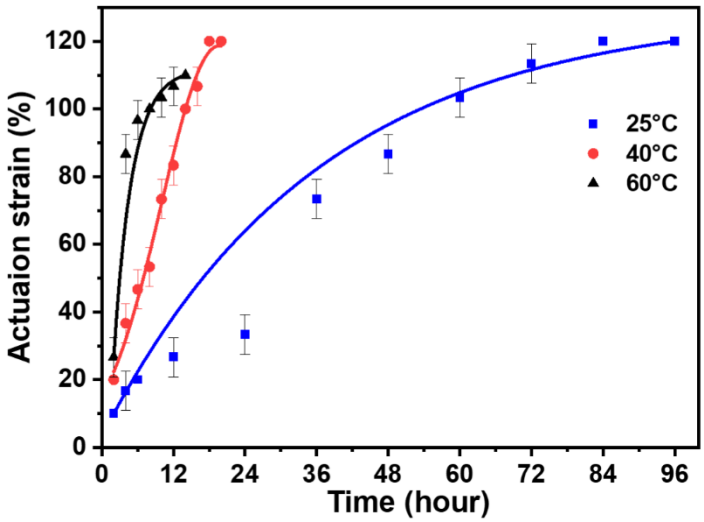

Supplementary Fig. 11 | Correlation between actuation strain and programming time at different temperatures. Error bars correspond to s.d. (n = 3).

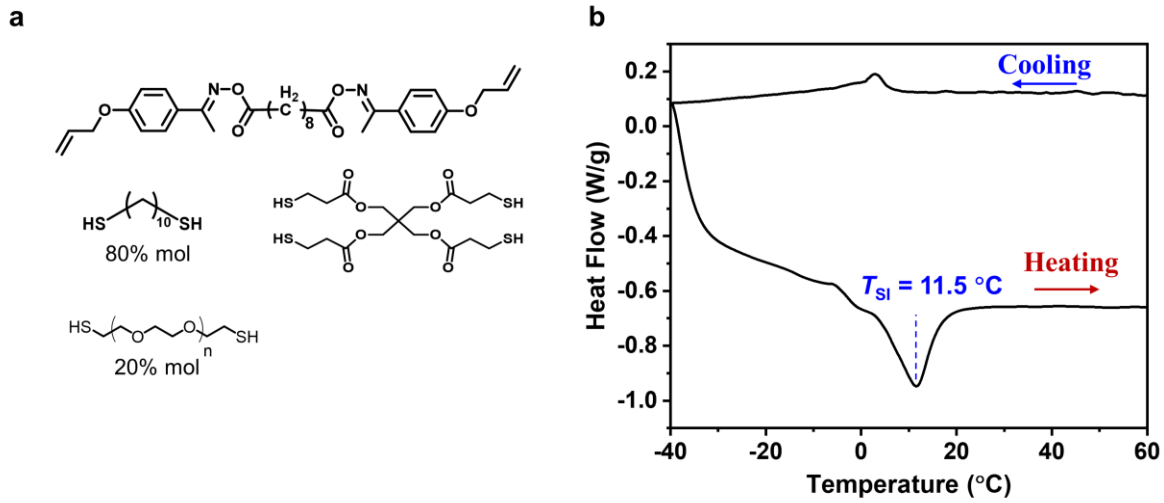

Supplementary Fig. 12 | Chemical formula and properties of self-rolling ice driven actuator (POE-L). **a**, Chemical structure of the monomers. **b,** DSC curves of POE-L actuator. We replaced part of the decanedithiol with 20% mol polyethylene glycol diol, which lowers the transition temperature to around 11 °C.

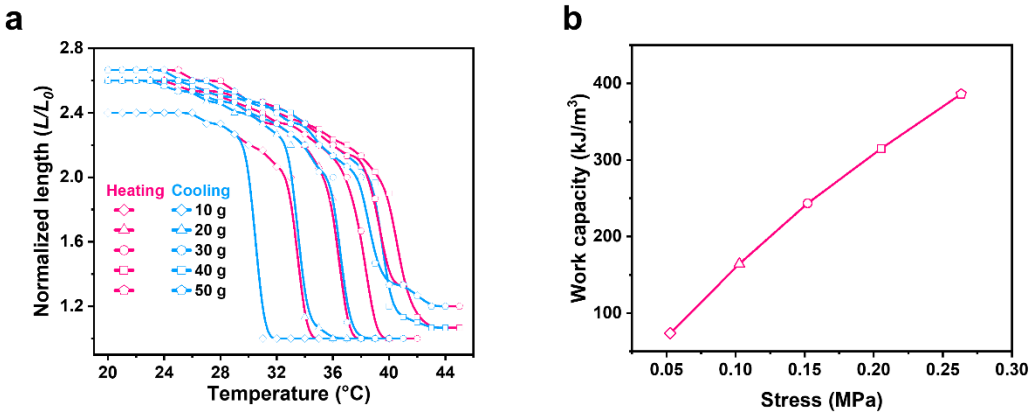

Supplementary Fig. 13 | Evaluation of mechanical work capacity generated during actuation under different stress. a, Strains vs temperature diagram of POE-6 film bearing a load from 10 gram to 50 gram. **b**, Corresponding work capacity of POE-6 under different stress.

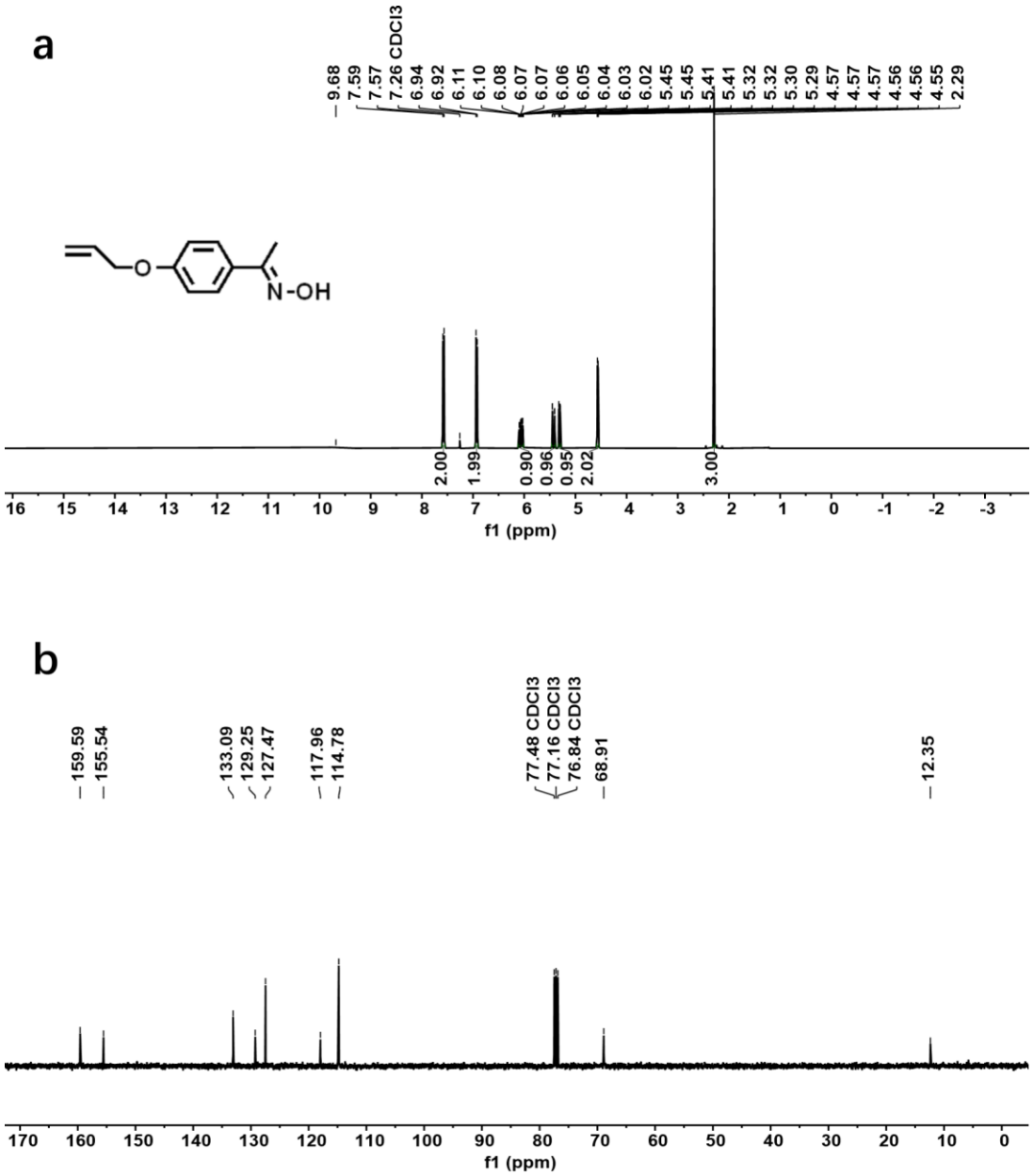

Supplementary Fig. 14 | a, ^{1}H NMR and b, ^{13}C NMR spectra of oxime. ^{1}H NMR (400 MHz, Chloroform-*d*) δ 7.58 (d, *J* = 8.9 Hz, 2H), 6.93 (d, *J* = 8.9 Hz, 2H), 6.06 (ddt, *J* = 17.3, 10.5, 5.3 Hz, 1H), 5.43 (dd, *J* = 17.3, 1.6 Hz, 1H), 5.31 (dd, *J* = 10.5, 1.4 Hz, 1H), 4.56 (dt, *J* = 5.3, 1.6 Hz, 2H), 2.29 (s, 3H). ^{13}C NMR (101 MHz, Chloroform-*d*) δ 159.59, 155.54, 133.09, 129.25, 127.47, 117.96, 114.78, 68.91, 12.35.

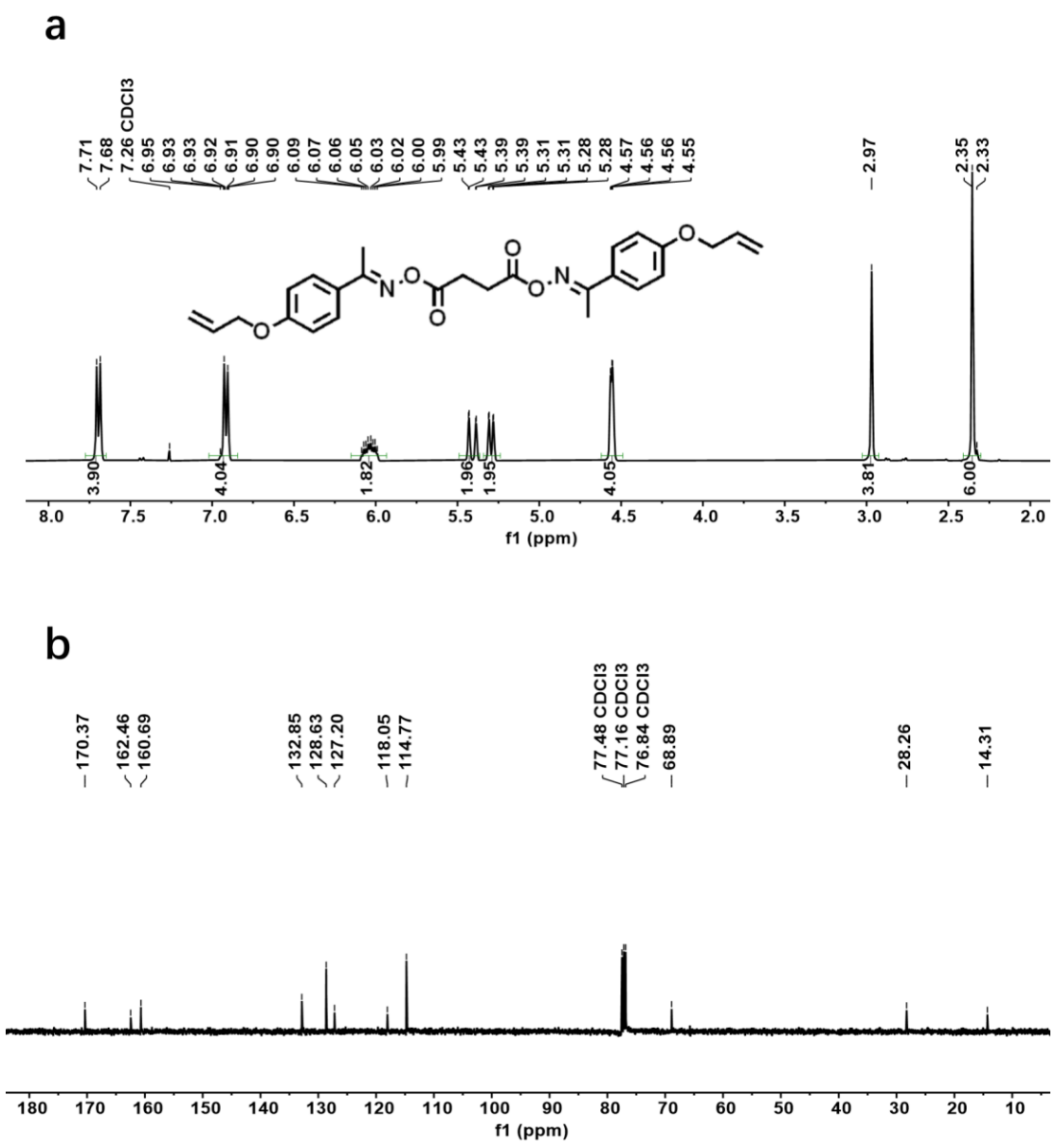

Supplementary Fig. 15 | a, ^{1}H NMR and b ^{13}C NMR spectra of oxime-ester-4. ^{1}H NMR (400 MHz, Chloroform-d) δ 7.70 (d, J = 8.9 Hz, 4H), 6.92 (dt, J = 9.1, 2.0 Hz, 4H), 6.04 (ddt, J = 15.8, 10.6, 5.3 Hz, 2H), 5.41 (dd, J = 17.2, 1.6 Hz, 2H), 5.30 (dd, J = 10.5, 1.6 Hz, 2H), 4.56 (dd, J = 3.6, 1.7 Hz, 4H), 2.97 (s, 4H), 2.35 (s, 6H). ^{13}C NMR (101 MHz, Chloroform-d) δ 170.37, 162.46, 160.69, 132.85, 128.63, 127.20, 118.05, 114.77, 68.89, 28.26, 14.31.

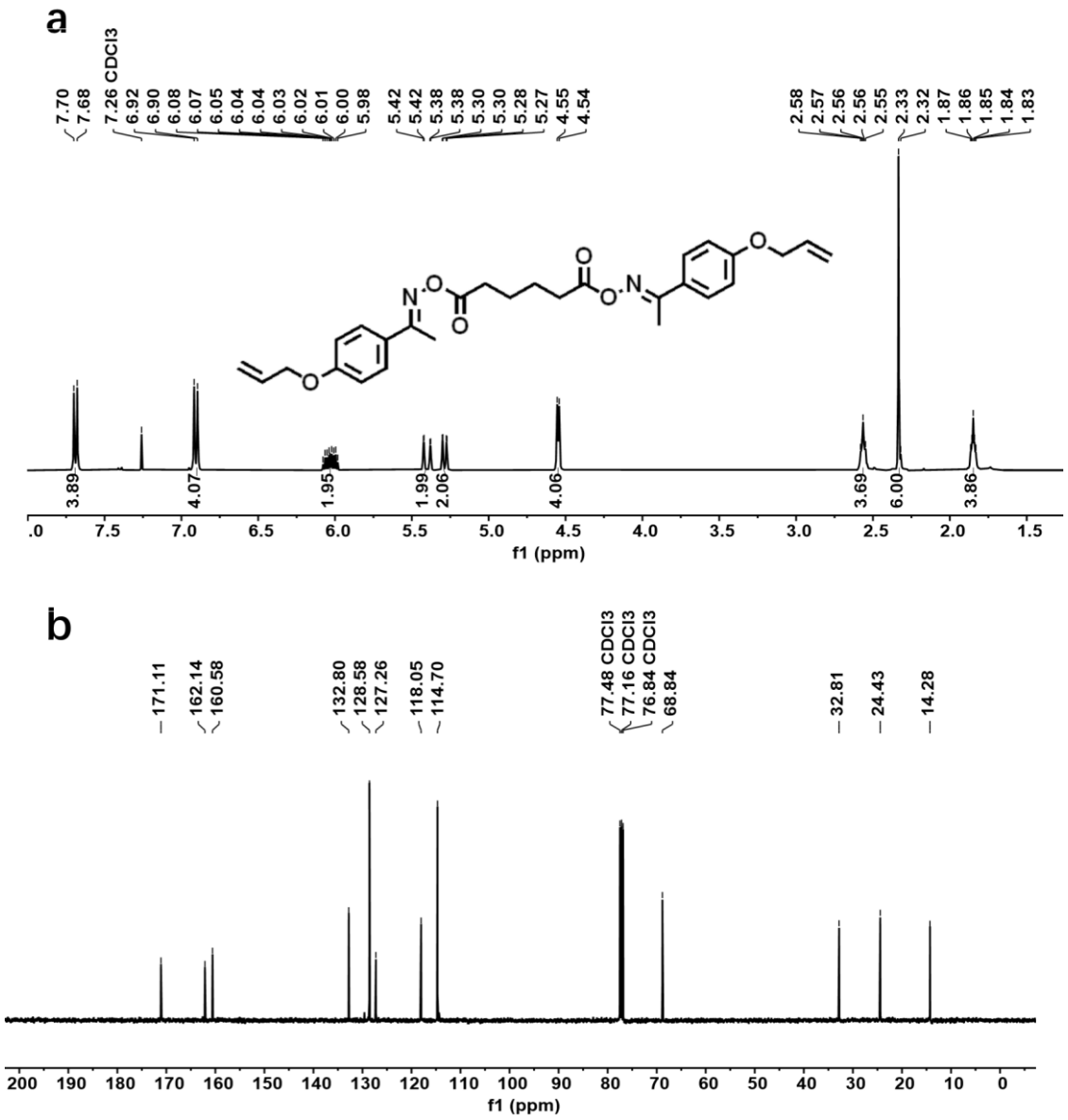

Supplementary Fig. 16 | a, ^{1}H NMR and b, ^{13}C NMR spectra of oxime-ester-6. ^{1}H NMR (400 MHz, Chloroform-d) δ 7.69 (d, J = 8.9 Hz, 4H), 6.91 (d, J = 8.9 Hz, 4H), 6.03 (ddt, J = 17.4, 10.5, 5.3 Hz, 2H), 5.40 (dd, J = 17.3, 1.7 Hz, 2H), 5.29 (dd, J = 10.5, 1.6 Hz, 2H), 4.55 (d, J = 5.3 Hz, 4H), 2.61 – 2.52 (m, 4H), 2.33 (s, 6H), 1.84 (h, J = 3.5 Hz, 4H). ^{13}C NMR (101 MHz, Chloroform-d) δ 171.11, 162.14, 160.58, 132.80, 128.58, 127.26, 118.05, 114.70, 68.84, 32.81, 24.43, 14.28.

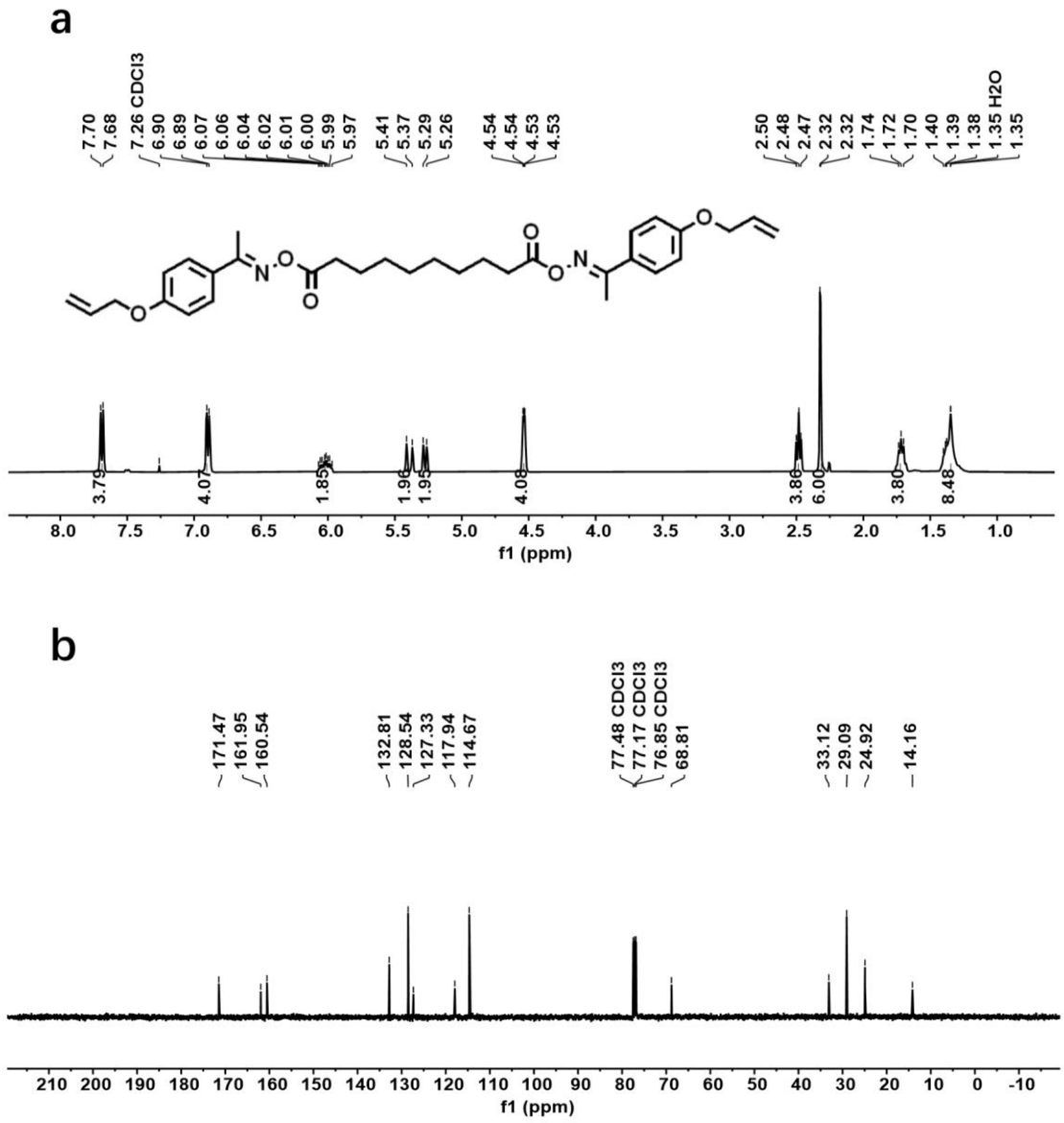

Supplementary Fig. 17 | a, ^{1}H NMR and b ^{13}C NMR spectra of oxime-ester-10. ^{1}H NMR (400 MHz, Chloroform-d) δ 7.69 (d, J = 7.0 Hz, 4H), 6.90 (d, J = 6.7 Hz, 4H), 6.09 – 5.95 (m, 2H), 5.39 (d, J = 17.3 Hz, 2H), 5.28 (d, J = 10.5 Hz, 2H), 4.54 (dd, J = 3.6, 1.7 Hz, 4H), 2.48 (t, J = 6.7 Hz, 4H), 2.32 (d, J = 2.1 Hz, 6H), 1.79 – 1.66 (m, 4H), 1.45 – 1.24 (m, 8H). ^{13}C NMR (101 MHz, Chloroform-d) δ 171.47, 161.95, 160.54, 132.81, 128.54, 127.33, 117.94, 114.67, 68.81, 33.12, 29.09, 24.92, 14.16.

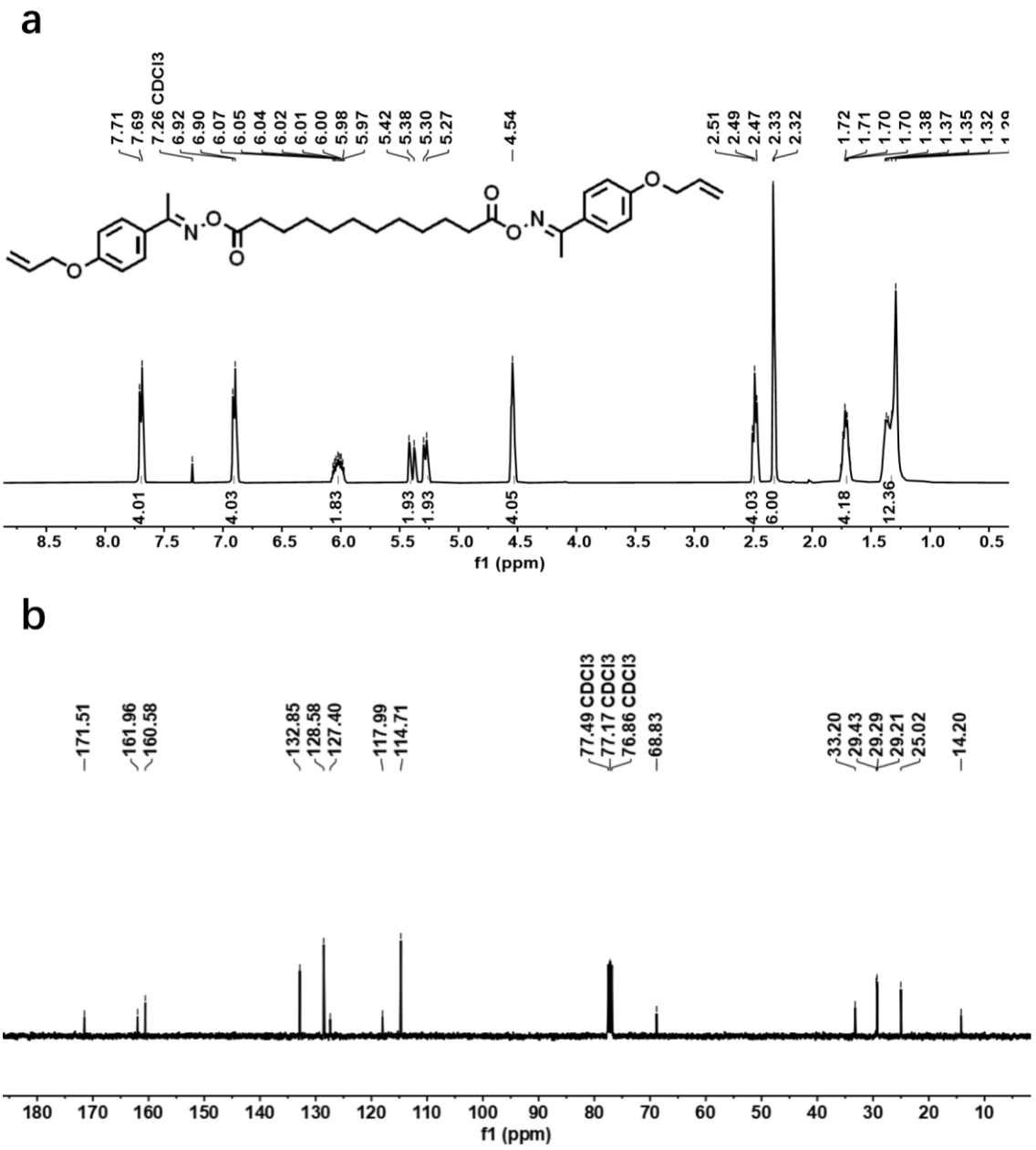

Supplementary Fig. 18 | a, ^{1}H NMR and b ^{13}C NMR spectra of oxime-ester-12. ^{1}H NMR (400 MHz, Chloroform-*d*) δ 7.70 (d, *J* = 8.7 Hz, 4H), 6.91 (d, *J* = 8.6 Hz, 4H), 6.02 (ddp, *J* = 14.8, 9.8, 5.2 Hz, 2H), 5.40 (d, *J* = 17.3 Hz, 2H), 5.28 (d, *J* = 10.4 Hz, 2H), 4.54 (s, 4H), 2.49 (t, *J* = 7.4 Hz, 4H), 2.33 (d, *J* = 3.5 Hz, 6H), 1.80 – 1.62 (m, 4H), 1.33 (d, *J* = 31.8 Hz, 12H). ^{13}C NMR (101 MHz, Chloroform-*d*) δ 171.51, 161.96, 160.58, 132.85, 128.58, 127.40, 117.99, 114.71, 68.83, 33.20, 29.43, 29.29, 25.02, 25.02, 14.20.

Supplementary Table 1 | Comparison of the modulus and threshold stress of nematic, smectic liquid crystal elastomer, and POE-6.

	Nematic[a]	**Smectic[b]**	**POE-6 (this work)**
Modulus of the initial elastic region E_1 **(MPa)**	**0.1~5**	**1~20**	**0.11**
Threshold stress to enter the soft plateau σ_s **(MPa)**	**0.01~0.2**	**0.2~5**	**0.05**

[a]reference 1-4; [b]reference 5-7

Supplementary Table 2 | Comparison of the actuation strain and actuation temperature for conventional LCEs.

Monomers	Actuation strain[a] (%)	Actuation temperature (°C)	Reference
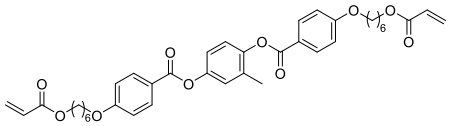 RM 82	37	65	*28*
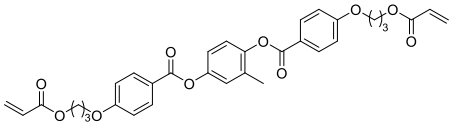 RM257	33	42	*29*
	50	53.2	*30*
RM 82 and RM 257	59	45.8	*31*
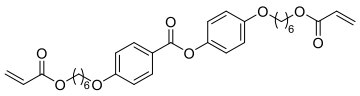 C6BAPE	89	59	*13*
C6BAPE and RM 257	53.8	11	*12*
	61	32	*32*
C6BAPE and RM 82	73.8	60	*33*
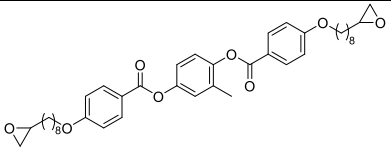 LC expoxy monomer	61	60.1	*34*
RM257	50	40	*35*
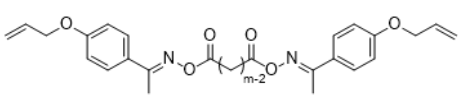 Oxime ester-*m*	132	33	This work
	100	11.5	

[a] The actuation strain was recalculated from the data in the references using an identical equation: actuation strain= $(L_{cold} - L_{heat})/L_{heat} \times 100\%$, where L_{cold} and L_{heat} represent the strains below and above the liquid crystalline transition temperature, respectively.

Supplementary Table 3 | The components of POE-*m* with varying oxime-ester-*m*. The molar ratios of -SH to –C=C group(1:1) are fixed.

Samples	Oxime-ester-*m*	Dithiol	PETMP
Linear POE-6	1.0 g 2.03 mmol	0.5 g 2.44 mmol	/
POE-4	0.83 g 1.79 mmol	0.2 g 0.97 mmol	0.2 g 0.41 mmol
POE-6	0.88 g 1.79 mmol	0.2 g 0.97 mmol	0.2 g 0.41 mmol
POE-10	0.98 g 1.79 mmol	0.2 g 0.97 mmol	0.2 g 0.41 mmol
POE-12	1.03 g 1.79 mmol	0.2 g 0.97 mmol	0.2 g 0.41 mmol

Supplementary Table 4 | Comparison of the work capacity, actuation strain and actuation temperature of LCE reported in the literature and POE-6.

Sample	Work Capacity (kJ m^{-3})	Actuation strain (%)	Actuation Temperature (℃)
POE-6	**386**	**147**	**45**
Ref. 8	1427	45	120
Ref. 9	1267	40	140
Ref. 10	730	87	150
Ref. 11	440	82	83
Ref. 12	~160	32	90
Ref. 13	100	12	120
Ref. 14	262	525	150
Ref. 15	140	40	130
Ref. 16	102	32	110

Reference

1. Saed, M. O. *et al.* Impact damping and vibration attenuation in nematic liquid crystal elastomers. *Nat. Commun.* **12** (2021).
2. Lu, H.-F., Wang, M., Chen, X.-M., Lin, B.-P. & Yang, H. Interpenetrating Liquid-Crystal Polyurethane/Polyacrylate Elastomer with Ultrastrong Mechanical Property. *J. Am. Chem. Soc.* **141**, 14364-14369 (2019).
3. Merkel, D. R., Traugutt, N. A., Visvanathan, R., Yakacki, C. M. & Frick, C. P. Thermomechanical properties of monodomain nematic main-chain liquid crystal elastomers. *Soft Matter* **14**, 6024-6036 (2018).
4. Raistrick, T. *et al.* Resolving the mechanical response of liquid crystal elastomers – semi-soft elastic or auxetic. *Soft Matter* **21**, 8849-8866 (2025).
5. Aßfalg, N., Finkelmann. H. A Smectic A liquid single crystal elastomer (LSCE): phase behavior and mechanical anisotropy. *Macromol. Chem. Phys.* **202**, 794-800 (2001).
6. Patil, H. P., Lentz, D. M., Hedden, R. C. Necking instability during polydomain-monodomain transition in a smectic main-chain elastomer. *Macromolecules* **42**, 3525-3531 (2009).
7. Amela-Cortés, M., Bruce, D. W., Evans, K. E. & Smith, C. W. Unsymmetric main-chain liquid crystal elastomers with tunable phase behaviour: elastic response. *J. Mater. Chem.* **21** (2011).
8. Li, C. *et al.* Enabling ultra-high work capacity and scalable processability of liquid crystal actuators through densely entangled structures. *Adv. Mater.* **38** (2026).
9. Lu, H. F. *et al.* Interpenetrating liquid-crystal polyurethane/polyacrylate elastomer with ultrastrong mechanical property. *J. Am. Chem. Soc.* **141** (2019).
10. Kim, H. *et al.* Tough, Shape-changing materials: crystallized liquid crystal elastomers. *Macromolecules* **50** (2017).
11. Ding, J. *et al.* Locking alignment of liquid crystal actuators using hydrogen bonds to enable room-temperature shape programmability and enhanced work capacity. *Adv. Fun. Mater.* **35** (2024).
12. Li, S. *et al.* Digital light processing of liquid crystal elastomers for self-sensing artificial muscles. *Sci. Adv.* **7** (2021).
13. Kim, H. *et al.* Intelligently actuating liquid crystal elastomer-carbon nanotube composites. *Adv. Fun. Mater.* **29** (2019).
14. Saed, M. O. *et al.* High strain actuation liquid crystal elastomers via modulation of mesophase structure. *Soft Mater.* **13** (2017).
15. Lugger, S. J. D. *et al.* One-pot synthesis of melt-processable supramolecular soft actuators. *Angew. Chem.* **61** (2022).
16. Lee, J. H. *et al.* Robust and reprocessable artificial muscles based on liquid crystal elastomers with dynamic thiourea bonds. *Adv. Fun. Mater.* **32** (2021).